scientific reports

Check for updates

OPEN

Spatiotemporal variability of hydro-meteorological droughts over the Arabian Peninsula and associated mechanisms

Md Saquib Saharwardi[1,2], Hari Prasad Dasari[1,2], Harikishan Gandham[1,2], Karumuri Ashok[1,2] & Ibrahim Hoteit[1]✉

This study examines the spatiotemporal variability of drought and associated physical processes over the Arabian Peninsula (AP). For this purpose, we computed the standardized precipitation evapotranspiration index (SPEI) for the period 1951–2020 using the Climate Research Unit and fifth generation ECMWF atmospheric reanalysis datasets. By applying rotated empirical orthogonal function analysis on the SPEI data, we identified four homogeneous and coherent drought regions. The droughts in the northern regions follow a relatively similar temporal evolution as compared to those in the southern region. All four sub-regions of the AP exhibit a significant drying trend ($p < 0.01$) with an abrupt acceleration in drought frequency and intensity over the last two decades. The increase in droughts is associated with the reduction of synoptic activity and an increase in the high pressure over the AP. Seasonally, potential evapotranspiration is the dominant driver of summer droughts in the AP, whereas both precipitation and temperature are important for driving winter droughts. The summer droughts, mainly over the northern AP, are due to the occurrence of an anomalous equivalent barotropic high associated with anomalous dry and hot conditions. However, anomalous dry conditions in winter are a result of an anomalous paucity of winter storms caused by the weakening of the sub-tropical jets.

Drought is a long-lasting, devastating environmental disaster driven by a hydrological imbalance caused by complex interactions between dynamical and thermodynamical processes[1]. A drought event is normally triggered by a meteorological phenomenon associated with prolonged precipitation deficit and excessive evapotranspiration. A drought that leads to decreased soil moisture is referred to as an agricultural drought[2,3]. Hydrological droughts are those that cause a significant reduction in surface and sub-surface water availability[2]. The complex nature and spatiotemporal variability of droughts have detrimental impacts on water resources. Drought's frequency and severity have increased during the global warming era[4,5] and are generally expected to intensify in the future[6,7]. However, their regional manifestations may vary due to the variations and changes in their large-scale drivers, regional dynamics, and land surface conditions, in addition to human interventions[8].

A case in point is the Arabian Peninsula (AP), comprising seven countries, which is a hot desert and an exceptionally water-stressed region (Fig. 1)[9].

The highest temperatures over the northern AP occur during summer (May–Oct) and the lowest temperatures occur during winter (Nov–Apr) in the southwestern region, due to land-sea interactions[10,11]. Most of the AP receives low precipitation mainly during winter season[11,12]. This winter precipitation is mainly due to the cold cyclonic systems that move eastward from the Mediterranean along the subtropical and polar jet streams[11,13]. Conversely, the southwest mountainous regions of the AP also receive some precipitation during summer, resulting from the orographic lifting of the monsoonal circulation, which is essentially an extension of the African monsoon[13,14]. These diverse spatiotemporal hydroclimatic patterns suggest that droughts should also be studied at sub-regional scales rather than addressing the whole AP region as a single entity. While sub-regions of drought have been identified for individual nations in the region[15,16] or in specific regions of individual interest[12]. To the best of our knowledge, no study has yet focused on identifying homogeneous drought regions for the whole AP.

[1]Physical Science and Engineering Division, King Abdullah University of Science and Technology, 23955-6900 Thuwal, Kingdom of Saudi Arabia. [2]Climate Change Center, National Center for Meteorology, 21431 Jeddah, Kingdom of Saudi Arabia. ✉email: ibrahim.hoteit@kaust.edu.sa

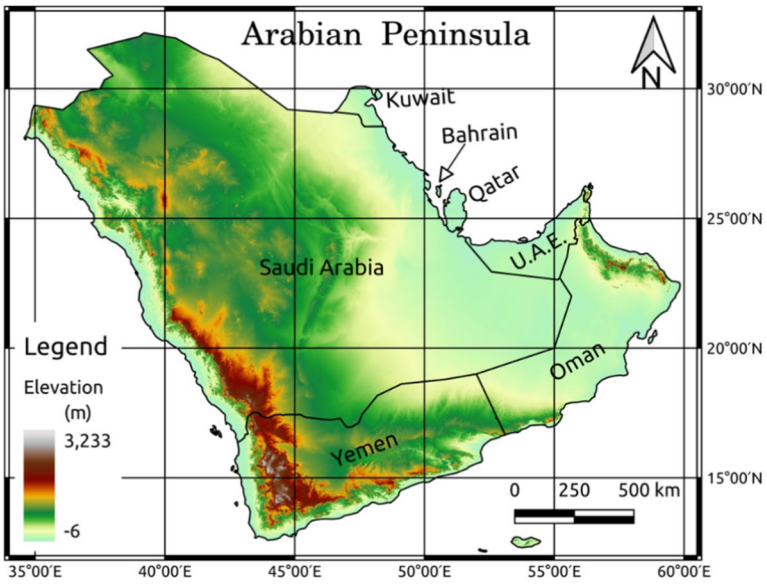

Fig. 1. Study area and topographical variations over the Arabian Peninsula.

Historically, droughts have caused mass migration and even civilization shifts in the AP[17–19]. The frequency of droughts has increased across most of the region in the recent few decades[19–21]. This increase accords with the increasing duration of summers over the same period[22] and a consistent upward trend in local temperatures[10,23]. Instead, trends in precipitation across the AP exhibit a degree of heterogeneity in spatiotemporal patterns[11,24,25]. Generally, droughts are attributed to precipitation deficits arising due to anomalous changes in atmospheric dynamics[26]. Another study suggested that the dryness over the AP in recent years is likely to be associated with weakening cyclonic and strengthening anticyclonic conditions[27]. However, previous studies suggest that potential evapotranspiration (PET)/temperature is a crucial for driving drought variability, which is associated with large-scale changes and feedback mechanism[28,29]. To date, studies have not examined the connections between the relative importance of hydrological drivers, such as precipitation and PET, and their seasonality and associated dynamical mechanisms for drought in the AP.

Several drought indices such as the standardized precipitation index (SPI)[30], palmer drought severity index (PDSI)[31], and standardized precipitation evapotranspiration index (SPEI)[32] have been used to analyze drought. Each index has its own advantages and limitations[2,33]. The SPI calculates multi-scalar drought features based on precipitation data[30], which potentially limits its application in arid regions because it only evaluates precipitation variability. The widely-used PDSI uses several parameters that are not readily accessible for long-term assessments[3,34]. It is also subject to several limitations; for example, it generally shows a lagged response for individual events and is only calculated for a single timescale[35]. The SPEI, which essentially depends on water balance, is a useful index to identify and catalog multi-scale droughts. As the concept of water balance is applicable to both high and low-rainfall regions, this index is appropriate for drought analysis over national or even sub-continental scales[32]. The actual computation of the SPEI involves PET derived from temperature, which makes it a suitable index to assess the drought conditions in dry and hot regions[36].

Considering the above knowledge gaps, this paper aims to: (1) identify homogeneous drought regions over the AP, (2) comprehensively examine the spatiotemporal variability of droughts during past and recent periods, and (3) understand the physical and dynamical processes associated with droughts. Below, "Dataset and methods" describes the datasets and methodology used, "Results" discusses the results, and "Discussion and conclusion" presents a summary and the conclusions of this study.

Dataset and methods

Datasets

We used the precipitation, near-surface temperature (mean, minimum, and maximum), and PET (version 4.00 TS4.05) datasets available at 0.5° × 0.5° spatial resolution for the period 1901–2020 from the Climate Research Unit (CRU), developed at the University of East Anglia[37]. These datasets were prepared using more than 4000 station measurements located around the globe and have been validated against station observations across the AP in several climate studies[10,11,27]. The CRU datasets were selected for use because they are quality controlled and available for the longest period with a reasonably high horizontal resolution.

We used the fifth-generation ECMWF Reanalysis (ERA5) dataset, which is the latest global atmospheric reanalysis available at 0.25° × 0.25° horizontal resolution available from the 1950s[38]. Several studies in Asia have deduced that ERA5 (hereafter ERA) outperforms other existing reanalysis and gridded products for hydroclimatic applications[39,40]. This dataset has also been used for climate studies over the AP[41,42]. In this study, we used the ERA precipitation and near-surface temperature (mean, minimum, and maximum) for the period 1951–2020.

We also used the ERA geopotential height (GPH), zonal, and meridional wind data at different pressure levels to understand potential physical mechanisms causing drought using the composite analysis technique.

We also analyzed the following two additional gridded datasets: the Global Precipitation Climatology Centre (GPCC) precipitation dataset at 0.5° × 0.5° for 1980–2019[43] and Multi-Source Weighted-Ensemble Precipitation (MSWEP) precipitation dataset at 0.25° × 0.25° for 1980–2019[44]. Both datasets have been used for the assessment of the observational uncertainty in precipitation datasets over the AP. Initially, we employed these four datasets to determine the best available gridded dataset for drought analysis in the AP. Among them, the ERA, GPCC, and MSWEP exhibited comparable performances (Table 1). Consequently, we opted for ERA due to its longer period availability, and as it includes essential variables like wind and geopotential data, which are crucial for studying drought-related physical mechanisms. In addition, we utilized the CRU dataset, derived from station measurements, for a comparative assessment. A detailed comparison of datasets is discussed in result. We bilinearly interpolated all the datasets to a common resolution for intercomparison.

Drought Index Calculation

We used the SPEI to represent the spatiotemporal variability of droughts based on ERA and CRU datasets in the AP because temperature is a major climate variable in addition to limited precipitation in the AP. The SPEI for a particular time period is defined as the normalized value of the aggregated water balance[32]. The water balance 'D' is obtained as the excess of the precipitation 'P' relative to the PET.

Thereafter, water balance is subtracted from the precipitation aggregated over different timescales,

$$D_n^k = \sum_{i=0}^{k-1} .(P_{n-i} - PET_{n-i}), n \geq k \tag{1}$$

where n is the time period and k (months) is the aggregation timescale. The 'D' values are undefined for k > n.

It is important to note that the choice of the distribution for fitting the SPEI is crucial[45,46]. In this study, we compared five well-known distributions to fit the water balance parameter (D). Our analysis indicates a nearly consistent agreement regardless of the distribution choice when fitting the water balance parameter (D) (see Table S1). The log-logistic distribution exhibited the lowest sum of squared error and Kolmogorov–Smirnov (KS) statistic, confirming its suitability for SPEI across the AP (see Table S1). The result is in line with the findings reported in the well-known paper by Vicente-Serrano et al. (2010) for estimating the SPEI[32]. The PDF of the D series as per log-logistic distribution is given by the following equation:

$$F(x) = \left[1 + \left(\frac{\alpha}{D - \gamma}\right)^{\beta}\right]^{-1} \tag{2}$$

where, α, β, and γ are the respective scale, shape, and origin parameters of the distribution.

The SPEI is obtained as the standardized value of F(x) as given by the equation below,

$$\text{SPEI} = \text{W} - \frac{C_0 + C_1 W + C_2 W^2}{1 + d_1 W + d_2 W^2 + d_3 W^3} \tag{3}$$

where $W = \sqrt{-2ln(P)}$ for $P \leq 0.5$, and P is the probability of exceeding a given D value, P = 1 − F(x). If P is greater than 0.5, P is replaced by 1 − P, and the sign of the resulting SPEI is reversed. $C_0 = 2.515517$, $C_1 = 0.802853$, $C_2 = 0.010328$, $d_1 = 1.432788$, $d_2 = 0.189269$, and $d_3 = 0.001308$ are the constants.

Several methods exist for calculating PET[47]. The most recommended method, Penman–Monteith method[48], endorsed by the Food and Agriculture Organization (FAO) of the UN, requires several parameters such as wind speed, soil properties, temperature, pressure, and radiation. Unfortunately, many of these are often unavailable in long-term records[49]. Specifically for the AP region, to our knowledge, long term observations of radiation, soil moisture, etc. are unavailable. Because of this data limitation, implementing the PM method for the AP is not possible. Importantly, several studies have noted that both PM and Hargreaves approach[49] yield similar results[50]. Therefore, this study adopted the Hargreaves approach to estimate the PET using the equation:

$$PET = 0.0023 R_a \left(\frac{T_{max} + T_{min}}{2} + 17.8\right) \sqrt{T_{max} - T_{min}} \tag{4}$$

	1980–1997				1998–2020			
Period	ERA	CRU	GPCC	MSWEP	ERA	CRU	GPCC	MSWEP
ERA	1	0.85	0.83	0.96	1	0.28	0.82	0.91
CRU		1	0.75	0.82		1	0.06	0.26
GPCC			1	0.78			1	0.84
MSWEP				1				1

Table 1. Correlations between different precipitation datasets over the area-averaged AP for the period 1980–1997 and 1998–2020.

where T_{min} and T_{max} are the minimum, and maximum temperatures, respectively, and Ra is the extra-terrestrial radiation.

Further details for the calculation of SPEI are available in the original article[32]. Much of this study explores drought characteristics on a 12-month timescale, however, seasonal variability is also discussed. The drought severity scale for the SPEI is given in the Supplementary Material (see Table S2). We followed established criteria to identify droughts, which involves cataloging SPEI values below − 1 as drought and above 1 as wet[51–53]. These thresholds, and those for other categories, are detailed in Table S2. A count of the number of drought years under each category over the study period gives the frequency of the droughts in that category of severity.

Rotated EOF analysis

We applied a rotated empirical orthogonal function (REOF) analysis on the CRU based SPEI dataset for the period 1901–2020 to identify homogeneous drought regions. The equation for simple EOF is given below:

$$Z(x,y,t) = \sum_{k=1}^{N} FPC(t) * EOF(x,y) \tag{5}$$

where x is longitude, y is latitude, and t is time. The output has two components: PC is the timeseries variability, and EOF is the spatial pattern of different PC loadings.

The REOF calculation requires the specific number of PCs selected using the North rule of thumb, which uses the sampling error of each eigenvalue to ascertain non-degenerated EOFs[54,55]. The Varimax rotation method is applied to the selected PCs to find a more stable localized spatial pattern[56], aiming to reduce mode complexity by making large loadings larger and small loadings smaller. This method relaxes the spatial orthogonality constraint through linear transformation and yields a more generalized structure while maintaining the same temporal variability[57]. The choice of such orthogonal rotation is based on the notion of the energy for a specific point, which is influenced only by the surrounding points rather than all grid points in the entire domain. Several studies reported that identifying sub-regions based on REOF analysis could provide a more realistic regional representation of drought characteristics[35,55]. It is a useful method to identify localized phenomena such as droughts, which often persist beyond several seasons, and even years, and manifest due to multiple physical and dynamical drivers[58]; although it may not be appropriate for climate phenomena with large spatial variations[59]. Our analysis to identify homogeneous sub-regional droughts was performed on an annual scale because droughts persist beyond a season. In addition, we repeated the analysis at a seasonal scale to identify distinctions between short-term and long-term droughts over the AP. We also applied this methodology on $SPEI_{CRU}$ and $SPEI_{ERA}$ dataset for the period 1951–2020 for comparison (see Supplementary Fig. S1).

Additional statistical analysis

We have applied Modified Mann–Kendall (MMK) test to identify trends in the droughts timeseries[60]. Importantly, the MMK test accounts for autocorrelation in the climate data timeseries. Pearson correlation analysis was used to determine the association between the variables examined in this study. We identified abrupt changes in SPEI variability using the Change Point Model (CPM)[61], which has been used in hydroclimatic studies to detect multiple change points in a single timeseries[35,62]. The CPM method involves processing an entire sequence of observations, for example, a timeseries of precipitation at a grid-point. Using a non-parametric Bartlett's method of the CPM[63], we have tested whether a change point statistically occurred in the mean of the timeseries. Additionally, we computed the transient activity over the AP in terms of the root mean square of 2–10 days Lanczos bandpass filtered 200 hPa GPH[64]. Statistical significance is given at 95% confidence level in all cases unless indicated otherwise. In this study, we mostly focused on the interannual drought variability, therefore, we selected the summer season of that particular dry year to identify dry summer. Similarly, to identify dry winter, we choose the winter season that starts from November of previous year to the following April. So, the years are common for both the seasons during dry or wet years. Similarly, we identified wet summer and wet winter. We used these dry and wet years to perform composite analysis.

Results

Homogeneous drought regions

The dominant four homogeneous drought regions over the AP obtained as resulting from the REOF analysis of annual SPEI are presented in Fig. 2. Together, these modes explained a variance of 83%. That these modes retain such a considerable proportion of variation is an important criterion for their selection as relevant patterns of dominant variability[35,54]. Importantly, the maximum loadings in the gravest four REOFs were concentrated in distinct quadrants (Fig. 2). The total variance explained by the gravest four modes of the EOF, as similar to REOF analysis (see Table S3). This shows that the identification of these top modes was robust, but the associated variance was more uniformly distributed among the top four REOF modes relative to the corresponding EOF modes. The loadings in each of the gravest four REOFs, except for REOF1, generally had a similar sign (Fig. 2). This, with the fact that the maximum loadings in each of the REOFs were located in distinct quadrants, suggests that these modes captured four homogeneous drought variability modes, with maximum variance related to a distinct quadrant of the AP. This allowed us to focus on the droughts in each of these maximized zones while also exploring any further homogeneity in the drought signal within the rest of the AP.

We defined four contiguous regions, each from one of the gravest REOF modes, and defined by a minimum loading of ~ 0.04, that contained the maximum SPEI variability. Given that these regions are located in four distinct quadrants, we designated these regions of maximum drought variance as the North West (NW), North East (NE), South West (SW), and South East (SE) drought regions (Fig. 2). Furthermore, correlations of the area-averaged SPEI in each of these regions were highest (> 0.9) with the RPC of the REOF that had the maximum

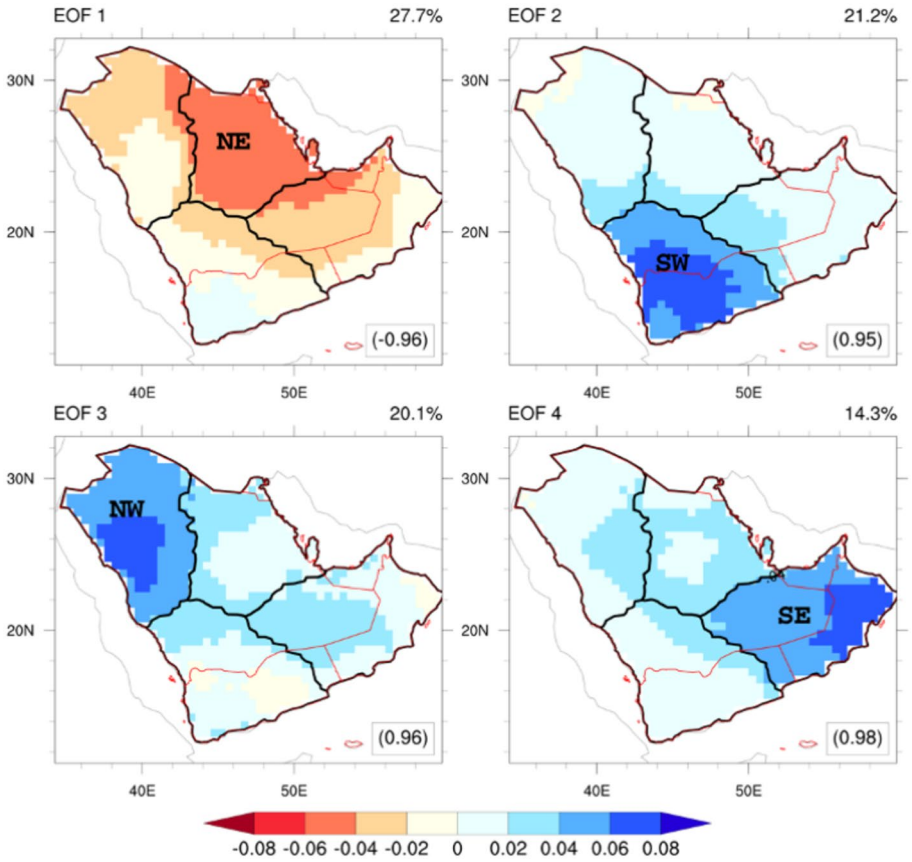

Fig. 2. Homogeneous drought regions over the AP identified using REOF analysis using the SPEI data for period 1901–2020. The corresponding PC values are shown in the upper right part of each figure. The lower right value indicates the correlation coefficient between RPC and the original SPEI dataset.

loading in that quadrant (see Supplementary Fig. S2), confirming that each REOF represented a separate homogeneous drought region. Interestingly, these homogeneous drought regions show some correspondence with previously identified regional precipitation patterns[16]. The homogenous regions obtained using the CRU data for the period 1901–2020 (Fig. 1) and 1951–2020 (see Supplementary Fig. S1a) reasonably matching with each other. Apart from this, the regions obtained from ERA for the period 1951–2020 also show good agreement with the homogenous regions identified for the CRU datasets over the 1951–2020 period as well as those for the longer period from 1901, except the fourth homogenous region (see Supplementary Fig. S1b). The drought characteristics and patterns over each of these homogeneous regions are discussed in the following section.

Drought variability over the AP and associated trends

The timeseries of the SPEI based on ERA (hereafter referred to as $SPEI_{ERA}$) area-averaged over the AP dataset over the longer time period (LTP) for 1951–2020 is shown in Fig. 3a. For comparison, we applied this analysis to the SPEI based on CRU (hereafter referred to as $SPEI_{CRU}$) (Fig. 3b). In addition, we carried out a similar analysis for the sub-period 1951–1997 (henceforth referred to as the SP1) and the sub-period 1998–2020 (henceforth referred to as the SP2), which we determined using CPM analysis. This allowed us to examine the sensitivity of the AP drought statistics to the choice of the datasets and study period. We observed that the interannual variability and long-term trends of SPEI at 03-month and 06-month and 12-month timescales, are similar (see Supplementary Fig. S3). Therefore, we focus on the droughts at 12-month scale, which also implicitly correspond to the variations in short term droughts. Both the $SPEI_{CRU}$ and $SPEI_{ERA}$ datasets showed a statistically significant decreasing trend across the LTP, albeit with differences in magnitude. However, this is misleading because both $SPEI_{CRU}$ and $SPEI_{ERA}$ exhibited a positive trend if only SP1 was considered; negative trends in the SPEI, indicating intensifying droughts, were only seen in SP2 (Fig. 3). The CPM application for each homogenous regions suggest an abrupt increase in drought near late 1990s. Although droughts have become more frequent in both datasets, distinctions across the two datasets were more prominent in SP2. Apart from this, the shift in drought activity over the AP is also visible from the SPI index, which is solely based on the precipitation dataset (Figure not shown). Specifically, trends in the $SPEI_{ERA}$ for the SP2 were opposite to those in the concurrent $SPEI_{CRU}$ (Fig. 3a,b). This apparent disagreement is because: (1) the CRU datasets indicate more frequent droughts for the period 1998–2020, and (2) although the CRU datasets indicate continuous droughts between 2015 and 2020, ERA datasets identify only two drought years, 2015, and 2017. However, there is reasonable agreement between the SPEI trends from both datasets for the period 1951–1997. Overall, the differences in the fluctuations within each

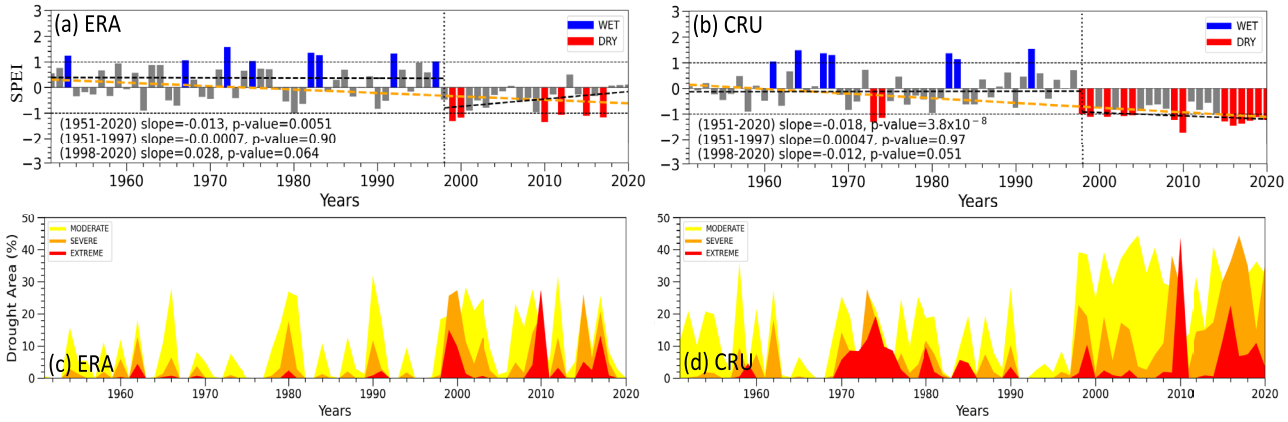

Fig. 3. (**a**, **b**) Interannual variability of $SPEI_{ERA}$ and $SPEI_{CRU}$ over the AP for the period 1951–2020. (**c**, **d**) Area affected by droughts based on severity levels for both $SPEI_{ERA}$ and $SPEI_{CRU}$ datasets. Red and blue colors with magnitudes equal or less than (more than) 1 represent drought and wet years, respectively.

sub-period may be subject to sampling and choice of datasets, unlike the robust signal of the long-term negative trend in the area-averaged SPEI over the AP. This is corroborated by the spatial distribution of long-term trends over the AP from both datasets (see Supplementary Fig. S4a,b). The discrepancies are discussed further below.

The changes in the percentage of the drought-affected area within the AP under different drought categories, using both $SPEI_{CRU}$ and $SPEI_{ERA}$, were investigated (Fig. 3c,d). Notwithstanding the discrepancies observed between the two datasets, drought affected areas increased in SP2 compared to SP1. During SP2, the area covered by all drought categories exhibited enhanced severity in $SPEI_{CRU}$ (~ 40%) and $SPEI_{ERA}$ (~ 30%). These discrepancies between the estimated drought-affected areas based on $SPEI_{ERA}$ and those from the $SPEI_{CRU}$ are largely due to differences in drought frequency and severity, as discussed earlier (Fig. 3a,b). In general, the area covered by moderate droughts is, understandably, higher compared to severe and extreme droughts in both sub-periods.

Further to the long-term weakening trend in the AP discerned from the area-averaged SPEI (Fig. 3a), all the homogeneous sub-regions displayed decreasing SPEI trends over the LTP (Fig. 4), irrespective of the datasets. CPM application for each homogenous regions suggest abrupt increase in drought near late 1990s. During the SP1, the SE, NE and NW homogeneous regions experienced increasing trends in the SPEI due to frequent wet events. In contrast, the SW region witnessed a drying trend (Fig. 4c,g). The continuous drought over the SW region for the period 1970–1980 in $SPEI_{CRU}$ subject to observational uncertainty (see Supplementary Fig. S5). However, over SP2, the evolution of the $SPEI_{CRU}$ and $SPEI_{ERA}$ over each homogeneous region suggested a dramatic increase in drought frequency and severity. Critically, no wet years were detected for any of the sub-regions in this sub-period, and the respective $SPEI_{CRU}$ and $SPEI_{ERA}$ values were mostly negative. The area-averaged SPEI time series using $SPEI_{ERA}$ and $SPEI_{CRU}$ based homogenous regions shows similar pattern, with a little difference in magnitude (see Supplementary Fig. S6 and Fig. 4).

Interestingly, interannual drought variations in both the northern homogeneous regions were highly correlated (0.89), which was significant at 99% confidence level two-tailed students t-test (see Supplementary Fig. S4c,d). Similarly, the variability of droughts in the two southern homogeneous regions was highly correlated (0.85). However, the association between the northern and southern regions was comparably weaker. Nonetheless, extreme droughts occurred in 1980, 1999, 2000, 2010, 2012, 2015, and 2017, affecting the entire AP with varying intensities (Fig. 4). For the LTP and SP1, there was a significant and high positive correlation between the $SPEI_{ERA}$ and $SPEI_{CRU}$ timeseries over all the homogeneous regions except the SW region (see Table S4). However, over SP2, there was a large discrepancy between the two timeseries in all the homogeneous regions (Fig. 3), discussed in the next section.

The potential cause of the differences in drought statistics across the datasets

The discrepancies between $SPEI_{ERA}$ and $SPEI_{CRU}$ in recent decades were primarily due to differences in the respective precipitation datasets. Temperatures over the AP from both datasets are strongly positively correlated (see Supplementary Fig. S5), and most of these are statistically significant at 95% confidence level two-tailed students t-test. During the SP2 sub-period, the area-averaged precipitation from the ERA was significantly positively correlated with the MSWEP and GPCC datasets for the same period (Table 1). On the other hand, the corresponding CRU precipitation area-averaged over the AP in SP2 was not significantly correlated with any other precipitation datasets (Table 1). What appears to be relatively extreme drought over the SW region over the period 1970–1980 in $SPEI_{CRU}$ is likely due to the quality issues of the CRU precipitation data (see Supplementary Fig. S5). The differences between the datasets highlight the relevance of observational uncertainty, which causes ambiguities in regional drought assessments. We have also demonstrated that the ambiguity in the CRU precipitation datasets mainly pertain to the SW region while comparing with ERA (see Supplementary Fig. S5). The CRU datasets are compared with station observations and show limitations for capturing the regional signal of precipitation variability over the SW region (Figure not shown).

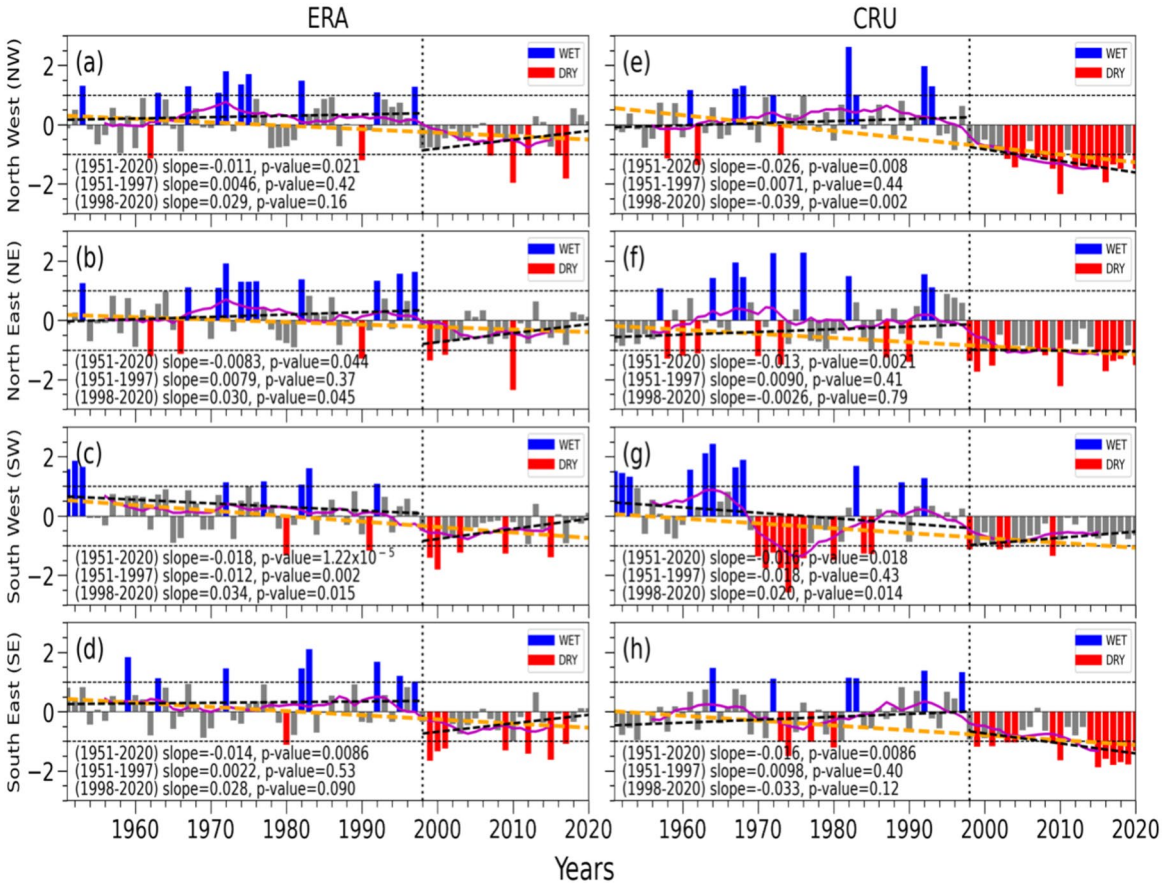

Fig. 4. Interannual variability of SPEI over each homogenous regions of AP for the period 1951–2020 based on (**a**–**d**) $SPEI_{ERA}$ and (**e**–**h**) $SPEI_{CRU}$ datasets.

Relative roles of precipitation and PET for driving droughts

To ascertain the respective importance of various physical drivers across the AP during dry (drought) versus wet years, we carried out a composite analysis of the anomalous precipitation for drought (Fig. 5a), which is a common feature for the whole AP based on ERA dataset (see Supplementary Figs. S3a and S7). The years 1999, 2000, 2010, 2012, 2015, 2017, shown in red color, were identified as drought years, and 1967, 1972, 1975, 1982, 1983, 1992, 1997, shown in blue color, as wet years (Fig. 3a). We also selected year 1962 and 1980, for composite analysis of droughts as these years also exhibits SPEI near to − 1. We also applied a similar composite analysis on the anomalous PET (Fig. 5d) and temperature patterns (Fig. 5g), and a similar analysis was repeated for the wet years. Finally, we repeated the composite analyses for the winter and summer seasons to obtain a seasonal perspective (see Supplementary Fig. S8).

The composite precipitation analysis showed significant negative anomalies during dry years (Fig. 5a) and positive anomalies over wet years (Fig. 5b) across the region, with largest differences over the SW region (Fig. 5c). On the other hand, composite analysis of temperature and PET suggested that drought years are associated with significantly higher temperatures (Fig. 5g) and positive PET (Fig. 5d), whereas wet years exhibited opposite signatures (Fig. 5e,h). The PET pattern largely coincided with the regional temperature anomalies during both dry and wet years (Fig. 5d–i), indicating the dominant contribution of temperature to PET. The contrasting relationship between precipitation and temperature has been observed in several previous studies[65,66].

Seasonally, a similar composite analysis of winter precipitation depicted stronger and significant differences between wet and dry years (see Supplementary Fig. S8). However, the magnitude of the corresponding differences in summer, and the areal extent of significant precipitation anomalies, were comparatively reduced except over the SW region near the coastal areas. The higher differences in precipitation during winter are due to the high magnitude of winter precipitation and its wider area coverage relative to the summer (see Supplementary Fig. S9). Furthermore, the differences in seasonal temperatures over the AP between the wet and dry seasons were strong, widespread, and significant in both seasons (see Supplementary Fig. S8). This was also reflected in the corresponding PET differences. Given the relative prominence and the wide areal extent of the temperature variations in both winter and summer over the AP, contributions of the PET to the long-term droughts will be more important relative to the precipitation changes.

Atmospheric conditions associated with droughts

Using composite analyses of atmospheric circulation and GPH at 500 hPa over the dry (drought) and wet years, we identified the large-scale circulation features that are associated with droughts over the AP. Our analysis of

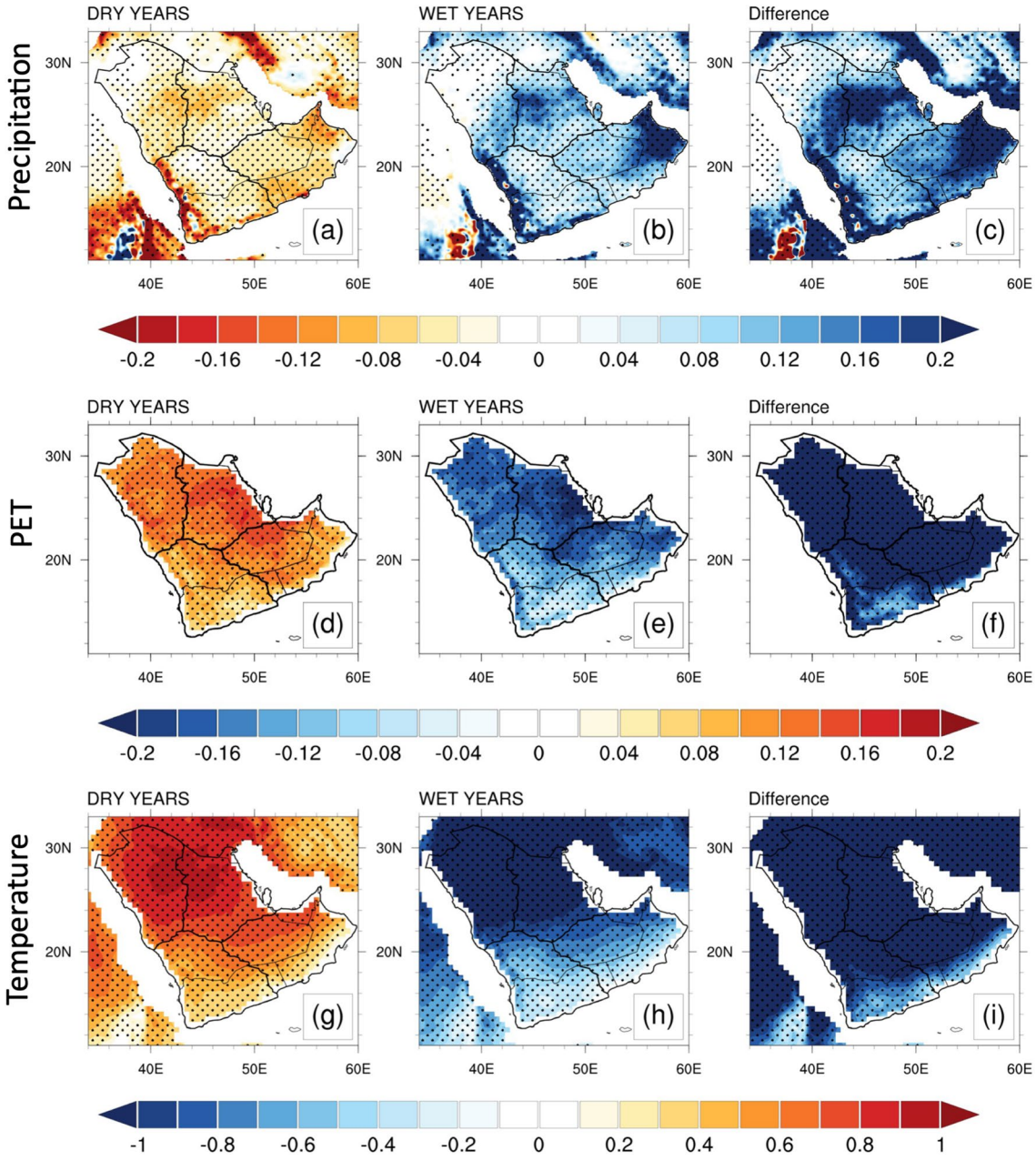

Fig. 5. Composite anomalies of mean precipitation (mm/day), PET (mm/day), and temperature (°C), and their differences during dry and wet years for the long-term period.

anomalous 500 hPa GPH composited over the dry summers during LTP suggested those dry summers were associated with an anomalous equivalent barotropic high that prevails over the northern AP (Fig. 6a). Interestingly, this pattern is an exacerbation of a band of anomalous high-pressure regions along 40° N. In particular, this anomalous barotropic high resulted in stronger anticyclonic winds over the AP during the dry years (Fig. 7b). Anomalous dry winds were stronger over Rub Al Khali (the greater Arabian desert), potentially leading to high dust extending to the southern Red Sea[67], enhancing dryness over the region. This summer circulation over the AP is also dominated by the evolution of the dry continental Shamal winds, which potentially enhance dryness over most of the AP region due to anomalously high temperatures (see Supplementary Fig. S8). The GPH at 500 hPa for wet years in both summer and winter seasons is opposite to that of dry years (Fig. 6b,d). In wet summers, the Shamal winds and the strength of the anticyclonic circulation over the northern AP are weaker compared to dry summers (Fig. 7a,c).

Climatologically, during winter, the Red Sea acts as a channel that transports moisture toward the north and central-north AP, causing precipitation over the majority of the region (Fig. 7d–f). This moisture transport pathway from the Red Sea depends on the position of the Arabian high over the AP[68,69]. An anomalous band of significant positive GPH anomalies at 500 hPa was observed stretching across the northern AP, from west to east, during dry winters (Fig. 6c), and are associated with anomalously high temperatures (see Supplementary Fig. S8).

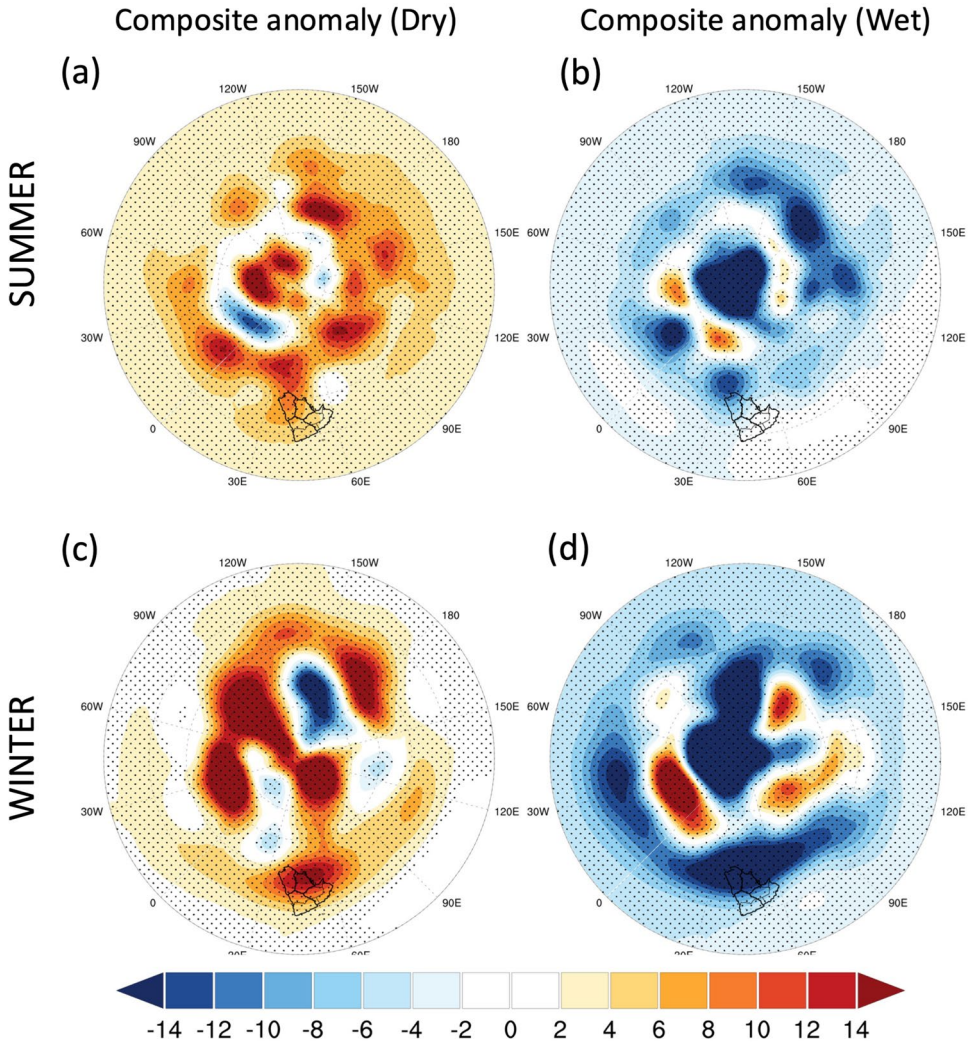

Fig. 6. Composite anomalies of geopotential height (m) at 500 hPa in summer and winter for dry and wet years, respectively.

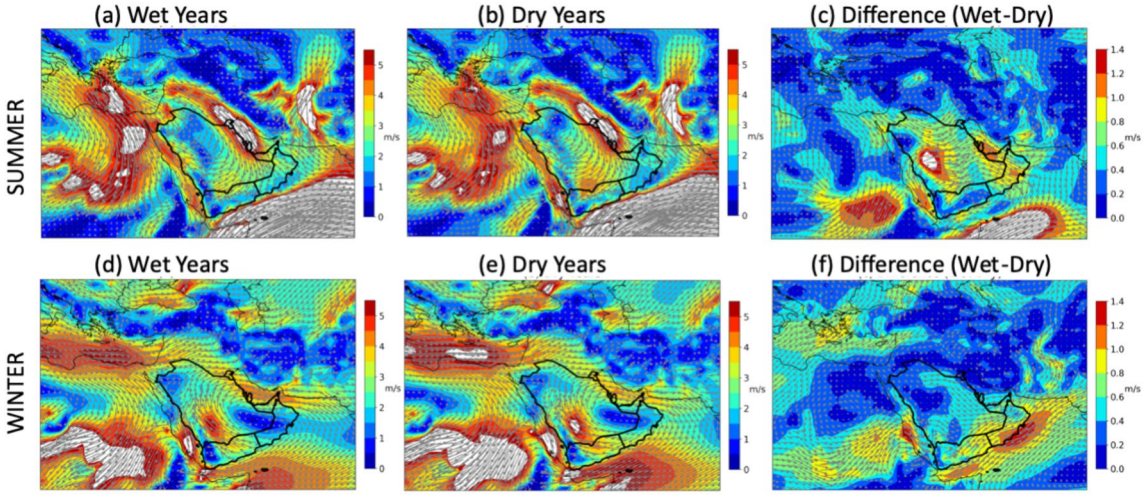

Fig. 7. Composite of mean atmospheric circulation (m/s) at 850 hpa during dry and wet years for summer and winter, respectively.

This region is the mean location of the storm tracks. Similar signatures were also seen at 200 hPa for GPH (see Supplementary Fig. S10), suggesting an equivalent barotropic high. Such a background signal in geopotential is accompanied by an anomalous weakening of the subtropical jet (Fig. 8a) and a weakening of the transient activity along the jet during dry winters (Fig. 8c). Overall, this suggests that the anomalous dry conditions are a result of an anomalous paucity of winter storms. On the other hand, during wet winters, we observed a band of anomalous low pressure over the AP, suggesting that the anomalous wet conditions were associated with higher synoptic storm track activity and a strengthened subtropical jet stream over the AP region (Fig. 8b,d).

Changes in atmospheric circulation features that accompany exacerbated droughts over the AP

We explored the decadal changes in atmospheric circulation, which have potentially facilitated a strengthening of droughts over the AP in recent decades. We focused on the winter season because most of the precipitation over the AP occurs in this season. In Fig. 9a,b, we show composites of anomalous GPH at 500 hPa over the winter droughts during the SP1 and SP2 sub-periods, respectively. We observed anomalous high pressure over most of the central and northern AP during both sub-periods, but the signal was much stronger during the SP2. This was also associated with substantially reduced transient activity over the AP during SP2 (Fig. 9c). Although, transient activity mostly occurs in winter, we also explored the transient changes in summer, which shows no signals of transient activity that can manifest the droughts (see Supplementary Fig. S11). Overall, this suggests that the exacerbated drought over the AP is associated with higher seasonal temperatures, reduced storm track activity, and relatively enhanced drying.

Discussion and conclusion

We investigated drought variability and associated physical processes over the AP for the period 1951–2020 by analyzing different reanalysis and observation based gridded datasets. The SPEI was chosen to represent drought variability because it accounts for variations in both precipitation and temperature, which is a dominant climate constraint in the desert region of the AP. We performed a comparative assessment of CRU and ERA datasets to analyze the drought spatiotemporal patterns over homogeneous drought regions of the AP. The rotated EOF

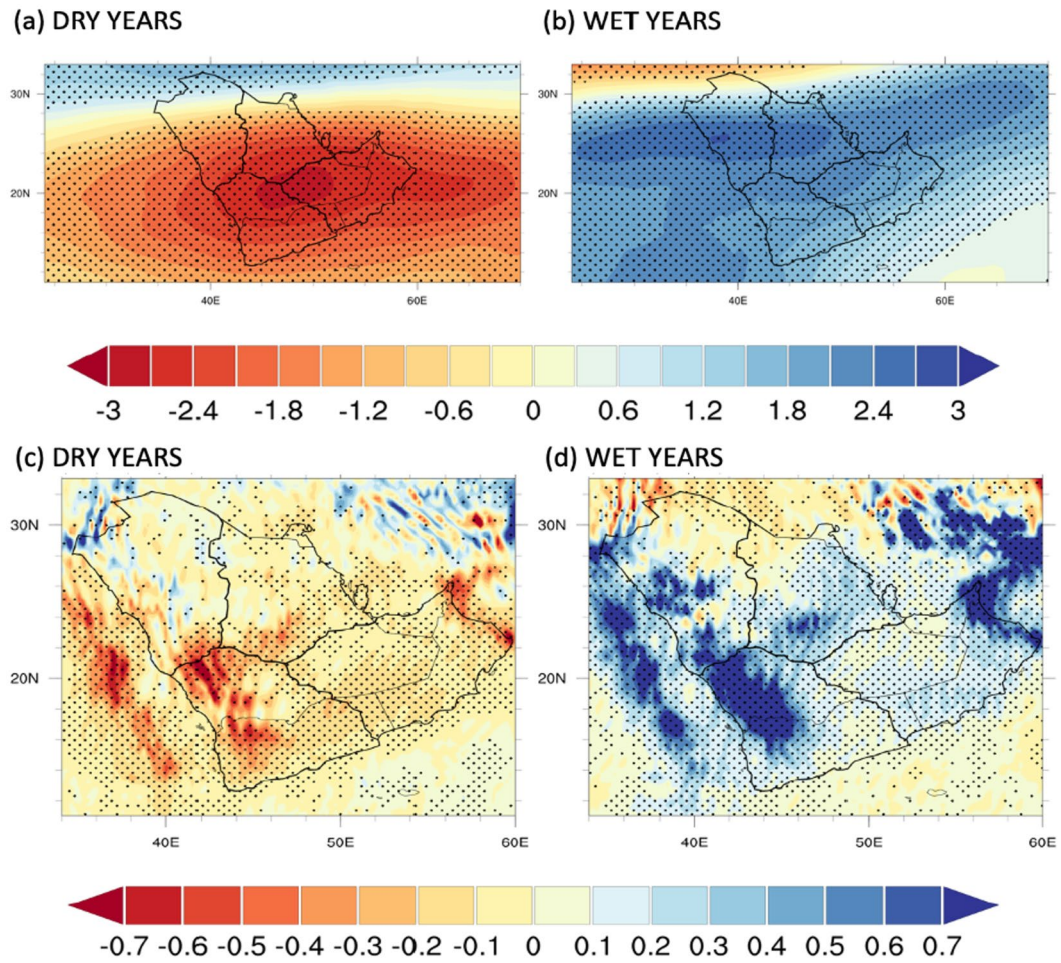

Fig. 8. (**a**, **b**) Composite anomalies of 200 hPa zonal wind over the AP in winter for dry and wet years. (**c**, **d**) Composite anomalies of transient activities over the AP in winter for dry and wet years.

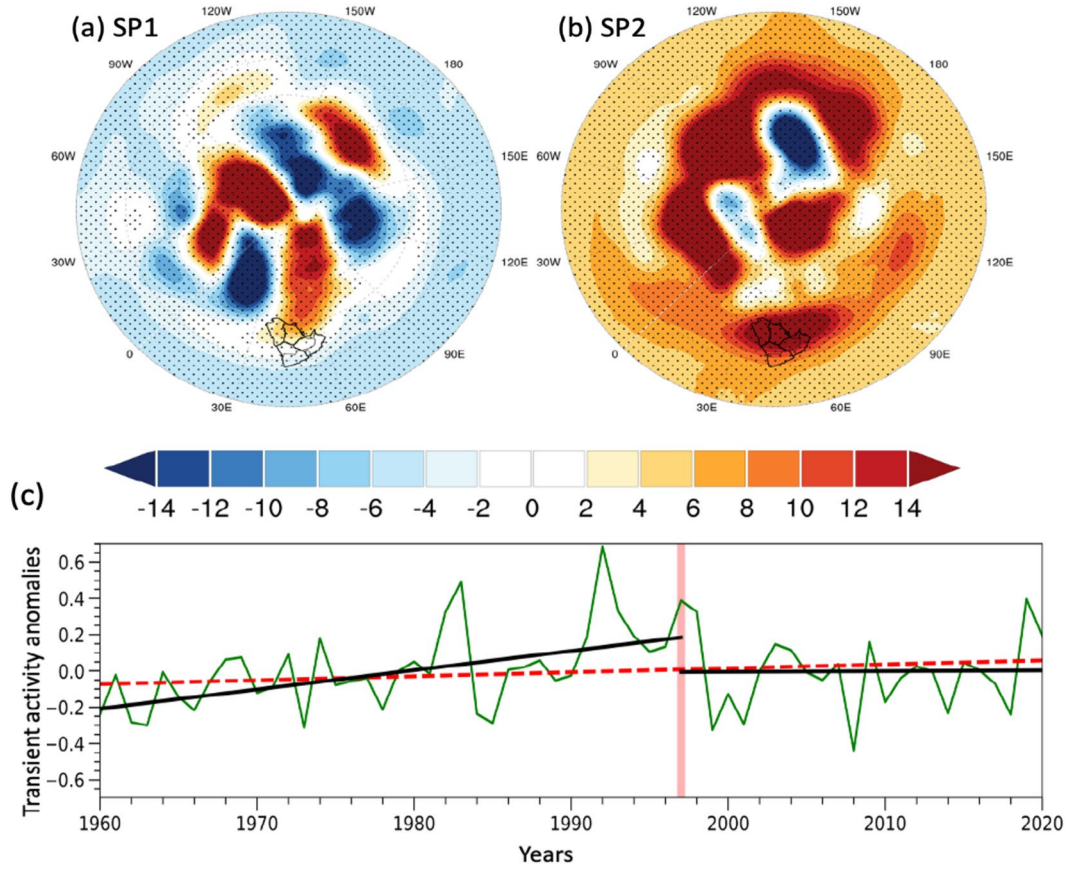

Fig. 9. (**a**, **b**) Composite anomalies of GPH at 500 hPa for drought years during SP1 and SP2. (**c**) Area-averaged transient activity anomalies over the AP for the period 1960–2020. The anomalies are calculated based on period 1960–2020.

analysis suggests that the AP has four homogeneous regions of drought, which we refer to as the NW, NE, SW, and SE regions. Interestingly, while we found a wetting trend over all the AP, except the SW region in the 1951–1997 period, a significant drying trend was observed in each of these four homogeneous regions over the longer period of 1951–2020, with an abrupt increase in drought frequency and severity in the most recent two decades. The frequent droughts in KSA and Oman in recent decades have also been reported previously[15,20,21,33,70].

The analysis of seasonal drought activity revealed the distinct roles of precipitation and PET (temperature) as drivers of droughts over the AP. During winter, both temperature and precipitation are major physical factors that drive drought activity over the AP. However, the potential evapotranspiration, which depends on temperature, is the dominant physical driver for summer drought due to the negligible precipitation across most of the AP, except for the SW mountainous region. Our results also show that winter droughts are a result of an anomalous northward shift of the subtropical jet and the anomalous paucity of winter storms caused by the weakening of the sub-tropical jets. On the other hand, summer droughts appear to be due to anomalous sub-tropical anticyclones over the AP region and are associated with an anomalous equivalent barotropic high over the northern AP, both resulting in anomalous dry and hot conditions. We also found that the exacerbation of droughts in recent decades is associated with a further reduction of synoptic activity and an enhanced increase in the high pressure over the AP relative to the previous years. Another recent study has also reported that these frequent drought over the AP is the manifestation of natural variability associated with Atlantic Multidecadal Oscillation[70].

Although both the $SPEI_{CRU}$ and $SPEI_{ERA}$ suggest an increase in drought frequency over the AP region if only the 1998–2020 period is considered, only the CRU dataset displays an increasing trend of droughts over the AP in this short period. This ambiguity is largely associated with the differences in precipitation between both datasets. Precipitation trends and variations over the southern AP depicted in the CRU datasets not only show significant differences to those from other datasets for this period but also with the station observations, however, ERA performs comparably with respect to station precipitation datasets (Figures not shown). Despite this limitation due to data uncertainty in the recent period over the southern AP, our results indicate long-term increasing trends in droughts. This needs to be factored in climate change adaptation plans for the AP and neighboring regions and is also critically important in validating the simulated global climate trends. This study is crucial in understanding the regional processes associated with the droughts. Such an understanding is also important to develop operational drought monitoring and forecasting systems for the AP.

In future studies, we will ascertain the proposed mechanisms for the manifestation of droughts and their recent increase over the AP, through model-based studies. Furthermore, the changes in the associated large-scale

driving forces due to anthropogenic warming[71] as well as natural variability[72], must be determined through an analysis of CMIP6 model projections and by performing sensitivity experiments with a high-resolution general circulation model suitable for the AP as necessary.

Data availability

All the datasets used in this study are publicly available freely from open sources. The CRU data is available from https://data.ceda.ac.uk/badc/cru/data/cru_ts/cru_ts_4.05/data. The pressure level ERA5 dataset is available to registered users at the Copernicus portal by https://cds.climate.copernicus.eu/cdsapp#!/dataset/reanalysis-era5-pressure-levels-monthly-means?tab=form, while single level ERA5 dataset was obtained from the link https://cds.climate.copernicus.eu/cdsapp#!/dataset/reanalysis-era5-single-levels-monthly-means?tab=form. The GPCC dataset was downloaded from https://psl.noaa.gov/data/gridded/data.gpcc.html, and MSWEP from http://www.gloh2o.org/mswep/.

Received: 8 September 2023; Accepted: 22 August 2024
Published online: 31 August 2024

References

1. Zhang, X., Obringer, R., Wei, C., Chen, N. & Niyogi, D. Droughts in India from 1981 to 2013 and implications to wheat production. *Sci. Rep.* **7**, 1–12 (2017).
2. Mishra, A. K. & Singh, V. P. Drought modelling—A review. *J. Hydrol.* **403**, 157–175 (2011).
3. Trenberth, K. E. *et al.* Global warming and changes in drought. *Nat. Clim. Chang.* **4**, 17–22 (2013).
4. Dai, A. Increasing drought under global warming in observations and models. *Nat. Clim. Chang.* **3**, 52–58 (2012).
5. Douville, H. *et al.* Water cycle changes. in *Climate Change 2021: The Physical Science Basis. Contribution of Working Group I to the Sixth Assessment Report of the Intergovernmental Panel on Climate Change* (Masson-Delmotte, V. *et al.* eds.), 1055–1210. (Cambridge University Press, 2021). https://doi.org/10.1017/9781009157896.010 (2021).
6. Sheffield, J. & Wood, E. F. Global trends and variability in soil moisture and drought characteristics, 1950–2000, from observation-driven simulations of the terrestrial hydrologic cycle. *J. Clim.* **21**, 432–458 (2008).
7. Naumann, G. *et al.* Global drought changes under high levels of warming. *Geophys. Res. Lett.* **13**, 2016–2051 (2016).
8. Van Loon, A. F. *et al.* Drought in a human-modified world: Reframing drought definitions, understanding, and analysis approaches. *Hydrol. Earth Syst. Sci.* **20**, 3631–3650 (2016).
9. Peel, M. C., Finlayson, B. L. & McMahon, T. A. Updated world map of the Köppen-Geiger climate classification. *Hydrol. Earth Syst. Sci.* **11**, 1633–1644 (2007).
10. Attada, R. *et al.* Surface air temperature variability over the Arabian Peninsula and its links to circulation patterns. *Int. J. Climatol.* **39**, 445–464 (2019).
11. Dasari, H. P. *et al.* Long-term changes in the Arabian Peninsula rainfall and their relationship with the ENSO signals in the tropical Indo-Pacific. *Clim. Dyn.* **1**, 1–17 (2021).
12. Almazroui, M. Calibration of TRMM rainfall climatology over Saudi Arabia during 1998–2009. *Atmos. Res.* **99**, 400–414 (2011).
13. Barlow, M. *et al.* A review of drought in the Middle East and Southwest Asia. *J. Clim.* **29**, 8547–8574 (2016).
14. Abid, M. A., Almazroui, M., Kucharski, F., O'Brien, E. & Yousef, A. E. ENSO relationship to summer rainfall variability and its potential predictability over Arabian Peninsula region. *NPJ Clim. Atmos. Sci.* **1**, 1–7 (2018).
15. El Kenawy, A. M. *et al.* Evidence for intensification of meteorological droughts in Oman over the past four decades. *Atmos. Res.* **246**, 105126 (2020).
16. Almazroui, M., Dambul, R., Islam, M. N. & Jones, P. D. Principal components-based regionalization of the Saudi Arabian climate. *Int. J. Climatol.* **35**, 2555–2573 (2015).
17. Kaniewski, D., Van Campo, E. & Weiss, H. Drought is a recurring challenge in the Middle East. *Proc. Natl. Acad. Sci. USA* **109**, 3862–3867 (2012).
18. Petraglia, M. D., Groucutt, H. S., Guagnin, M., Breeze, P. S. & Boivin, N. Human responses to climate and ecosystem change in ancient Arabia. *Proc. Natl. Acad. Sci. USA* **117**, 8263–8270 (2020).
19. Fleitmann, D. *et al.* Droughts and societal change: The environmental context for the emergence of Islam in late Antique Arabia. *Science* **80**(376), 1317–1321 (2022).
20. Almazroui, M. Assessment of meteorological droughts over Saudi Arabia using surface rainfall observations during the period 1978–2017. *Arab. J. Geosci.* **12**, 1–16 (2019).
21. Syed, F. S., Adnan, S., Zamreeq, A. & Ghulam, A. Identification of droughts over Saudi Arabia and global teleconnections. *Nat. Hazards*. **112**, 2717–2737 (2022).
22. Ajjur, S. B. & Al-Ghamdi, S. G. Seventy-year disruption of seasons characteristics in the Arabian Peninsula. *Int. J. Climatol.* **41**, 5920–5937 (2021).
23. Amin, M. T., Mahmoud, S. H. & Alazba, A. A. Observations, projections and impacts of climate change on water resources in Arabian Peninsula: Current and future scenarios. *Environ. Earth Sci.* **75**, 1–17 (2016).
24. Donat, M. G. *et al.* Changes in extreme temperature and precipitation in the Arab region: Long-term trends and variability related to ENSO and NAO. *Int. J. Climatol.* **34**, 581–592 (2014).
25. Hasanean, H. & Almazroui, M. Rainfall: Features and variations over Saudi Arabia. *A Review. Climate.* **3**, 578–626 (2015).
26. Erb, M. P., Emile-Geay, J., Hakim, G. J., Steiger, N. & Steig, E. J. Atmospheric dynamics drive most interannual US droughts over the last millennium. *Sci. Adv.* **6**, 7268–7275 (2020).
27. El Kenawy, A. M., McCabe, M. F., Stenchikov, G. L. & Raj, J. Multi-decadal classification of synoptic weather types, observed trends and links to rainfall characteristics over Saudi Arabia. *Front. Environ. Sci.* **2**, 37 (2014).
28. Diffenbaugh, N. S., Swain, D. L., Touma, D. & Lubchenco, J. Anthropogenic warming has increased drought risk in California. *Proc. Natl. Acad. Sci. USA* **112**, 3931–3936 (2015).
29. Mishra, V., Aadhar, S. & Mahto, S. S. Anthropogenic warming and intraseasonal summer monsoon variability amplify the risk of future flash droughts in India. *NPJ Clim. Atmos. Sci.* **4**, 1–10 (2021).
30. Mckee, T. B., Doesken, N. J. & Kleist, J. The relationship of drought frequency and duration to time scales. in *Eighth Conference on Applied Climatology* (1993).
31. Palmer, W.C. Meteorological Drought. Weather Bureau Research Paper No. 45. Washington, DC: US Department of Commerce (1965).
32. Vicente-Serrano, S. M., Beguería, S., López-Moreno, J. I., Angulo, M. & El Kenawy, A. A new global 0.5° gridded dataset (1901–2006) of a Multiscalar Drought Index: Comparison with current drought index datasets based on the Palmer Drought Severity Index. *J. Hydrometeorol.* **11**, 1033–1043 (2010).
33. Zargar, A., Sadiq, R., Naser, B. & Khan, F. I. A review of drought indices. *Environ. Rev.* **19**, 333–349 (2011).

34. Vicente-Serrano, S. M., Beguería, S. & López-Moreno, J. I. Comment on "Characteristics and trends in various forms of the Palmer Drought Severity Index (PDSI) during 1900–2008" by Aiguo Dai. *J. Geophys. Res. Atmos.* **116**, 19112 (2011).
35. Saharwardi, M. S., Kumar, P., Dubey, A. K. & Kumari, A. Understanding spatiotemporal variability of drought in recent decades and its drivers over identified homogeneous regions of India. *Q. J. R. Meteorol. Soc.* **148**, 2955–2972 (2022).
36. Vicente-Serrano, S. M. *et al.* Evidence of increasing drought severity caused by temperature rise in southern Europe. *Environ. Res. Lett.* **9**, 044001 (2014).
37. Harris, I., Jones, P. D., Osborn, T. J. & Lister, D. H. Updated high-resolution grids of monthly climatic observations—The CRU TS3.10 Dataset. *Int. J. Climatol.* **34**, 623–642 (2014).
38. Hersbach, H. *et al.* The ERA5 global reanalysis. *Q. J. R. Meteorol. Soc.* **146**, 1999–2049 (2020).
39. Mahto, S. S. & Mishra, V. Does ERA-5 outperform other reanalysis products for hydrologic applications in India?. *J. Geophys. Res. Atmos.* **124**, 9423–9441 (2019).
40. Zandler, H., Senftl, T. & Vanselow, K. A. Reanalysis datasets outperform other gridded climate products in vegetation change analysis in peripheral conservation areas of Central Asia. *Sci. Rep.* **10**, 1–16 (2020).
41. Bawadekji, A., Tonbol, K., Ghazouani, N., Becheikh, N. & Shaltout, M. Recent atmospheric changes and future projections along the Saudi Arabian Red Sea Coast. *Sci. Rep.* **12**, 1–19 (2022).
42. Safieddine, S., Clerbaux, C., Clarisse, L., Whitburn, S. & Eltahir, E. A. B. Present and future land surface and wet bulb temperatures in the Arabian Peninsula. *Environ. Res. Lett.* **17**, 044029 (2022).
43. Becker, A. *et al.* A description of the global land-surface precipitation data products of the Global Precipitation Climatology Centre with sample applications including centennial (trend) analysis from 1901 to present. *Earth Syst. Sci. Data* **5**, 71–99 (2013).
44. Beck, H. E. *et al.* MSWEP: 3-hourly 0.25° global gridded precipitation (1979–2015) by merging gauge, satellite, and reanalysis data. *Hydrol. Earth Syst. Sci.* **21**(1), 589–615 (2017).
45. Stagge, J. H., Tallaksen, L. M., Gudmundsson, L., Van Loon, A. F. & Stahl, K. Candidate distributions for climatological drought indices (SPI and SPEI). *Int. J. Climatol.* **35**, 4027–4040 (2015).
46. Wang, H. *et al.* Assessment of candidate distributions for SPI/SPEI and sensitivity of drought to climatic variables in China. *Int. J. Climatol.* **39**(11), 4392–4412 (2019).
47. Tabari, H., Grismer, M. E. & Trajkovic, S. Comparative analysis of 31 reference evapotranspiration methods under humid conditions. *Irrig. Sci.* **31**, 107–117 (2013).
48. Allen, R. G., Pereira, L. S., & Raes, D. Crop Evapotranspiration-Guidelines for computing crop water requirements-FAO Irrigation and drainage paper 56 Table of Contents, *FAO*, (1998). https://www.fao.org/4/X0490E/x0490e00.html
49. Hargreaves, G. H. & Samani, Z. A. Reference crop evapotranspiration from temperature. *Appl. Eng. Agric.* **1**, 96–99 (1985).
50. Kingston, D. G., Todd, M. C., Taylor, R. G., Thompson, J. R. & Arnell, N. W. Uncertainty in the estimation of potential evapotranspiration under climate change. *Geophys. Res. Lett.* **36**, L20403 (2009).
51. Kurniasih, E. et al. Use of Drought Index and Crop Modelling for Drought Impacts Analysis on Maize (Zea mays L.) Yield Loss in Bandung District, *IOP Conf. Ser.: Earth Environ. Sci.* 58 012036 (2017).
52. Li, B. *et al.* Using the SPEI to assess recent climate change in the Yarlung Zangbo River Basin, South Tibet. *Water* **7**, 5474–5486 (2015).
53. Yildirim, T., Moriasi, D. N., Starks, P. J. & Chakraborty, D. Using artificial neural network (ANN) for short-range prediction of cotton yield in data-scarce regions. *Agronomy* **12**, 828 (2022).
54. North, G. R. *et al.* Sampling errors in the estimation of empirical orthogonal functions. *Mon. Weather Rev.* **110**, 699–706 (1982).
55. Zambreski, Z. T., Lin, X., Aiken, R. M., Kluitenberg, G. J. & Pielke, R. A. Identification of hydroclimate subregions for seasonal drought monitoring in the US Great Plains. *J. Hydrol.* **567**, 370–381 (2018).
56. Kaiser, H. F. The varimax criterion for analytic rotation in factor analysis. *Psychometrika* **23**, 187–200 (1958).
57. Hannachi, A., Jolliffe, I. T., Stephenson, D. B. & Trendafilov, N. In search of simple structures in climate: Simplifying EOFs. *Int. J. Climatol.* **26**, 7–28 (2006).
58. Abatan, A. A. *et al.* Drivers and physical processes of drought events over the State of São Paulo, Brazil. *Clim. Dyn.* **58**, 3105–3119 (2022).
59. Behera, S. *et al.* Comments on "A Cautionary Note on the Interpretation of EOFs" *J. Clim.* **16**(17), 1087–1093 (2003).
60. Hamed, K. H. & Rao, A. R. A modified Mann-Kendall trend test for autocorrelated data. *J. Hydrol.* **204**(1–4), 182–196 (1998).
61. Ross, G. J. Parametric and nonparametric sequential change detection in R: The cpm package. *J. Stat. Softw.* **66**, 1–20 (2015).
62. Shirvani, A. Change in annual precipitation in the northwest of Iran. *Meteorol. Appl.* **24**, 211–218 (2017).
63. Bartlett, M. S. On the theoretical specification and sampling properties of autocorrelated time series. *Suppl. J. R. Stat. Soc.* **8**, 27–34 (1946).
64. Kang, I. S., Rashid, I. U., Kucharski, F., Almazroui, M. & Alkhalaf, A. K. Multidecadal changes in the relationship between ENSO and wet-season precipitation in the Arabian Peninsula. *J. Clim.* **28**, 4743–4752 (2015).
65. Zhao, W. & Khalil, M. A. K. The relationship between precipitation and temperature over the Contiguous United States. *J. Clim.* **6**, 1232–1240 (1993).
66. Trenberth, K. E. & Shea, D. J. Relationships between precipitation and surface temperature. *Geophys. Res. Lett.* **32**, 1–4 (2005).
67. Gandham, H., Dasari, H. P., Karumuri, A., Ravuri, P. M. K. & Hoteit, I. Three-dimensional structure and transport pathways of dust aerosols over West Asia. *NPJ Clim. Atmos. Sci.* **5**, 1–15 (2022).
68. De Vries, A. J. *et al.* Extreme precipitation events in the Middle East: Dynamics of the active red sea trough. *J. Geophys. Res. Atmos.* **118**, 7087–7108 (2013).
69. Dasari, H. P. *et al.* ENSO influence on the interannual variability of the Red Sea convergence zone and associated rainfall. *Int. J. Climatol.* **38**, 761–775 (2018).
70. Saharwardi, M. S., Dasari, H. P., Aggarwal, V., Ashok, K. & Hoteit, I. Long-term variability in the Arabian Peninsula droughts driven by the Atlantic Multidecadal Oscillation. *Earth's Fut.* **11**, 11 (2023).
71. Al Sarmi, S. & Washington, R. Recent observed climate change over the Arabian Peninsula. *J. Geophys. Res. Atmos.* **116**, 11109 (2011).
72. Ehsan, M. A. *et al.* Atlantic Ocean influence on Middle East summer surface air temperature. *NPJ Clim. Atmos. Sci.* **3**, 1–8 (2020).

Acknowledgements

This research was supported by the Climate Change Center, an initiative of the National Center for Meteorology (NCM), Kingdom of Saudi Arabia (Ref No: RGC/03/4829-01-01). We acknowledge the ECMWF for providing ERA5 products, CRU-UEA for CRU datasets, MSWEP, and GPCC for gridded precipitation datasets.

Author contributions

M.S.S. and I.H. took the overall lead in designing the current study. M.S.S. analyzed data and created all the figures. M.S.S. wrote the paper with help from I.H., K.A., H.P.D., and H.G. All authors participated in the review and editing.

Competing interests
The authors declare no competing interests.

Additional information
Supplementary Information The online version contains supplementary material available at https://doi.org/10.1038/s41598-024-70869-7.

Correspondence and requests for materials should be addressed to I.H.

Reprints and permissions information is available at www.nature.com/reprints.

Publisher's note Springer Nature remains neutral with regard to jurisdictional claims in published maps and institutional affiliations.